Contents lists available at ScienceDirect

Chemical Engineering Research and Design

journal homepage: www.elsevier.com/locate/cherd

Spray-coated tough thin film composite membrane for pervaporation desalination

Junli Wang, Bing Cao, Rui Zhang*, Pei Li**

College of Materials Science and Engineering, Beijing University of Chemical Technology, Beijing 100029, China

ARTICLE INFO

Article history:
Received 20 December 2021
Received in revised form 12 January 2022
Accepted 20 January 2022
Available online 28 January 2022

Keywords:
Pervaporation
Desalination
Composite membrane
Poly(vinyl alcohol)
Spray-coating

ABSTRACT

Water flux of pervaporation (PV) desalination membranes can be increased by reducing thickness of the selective layer and/or reducing the resistance of the support layer. However, low resistant support layer typically has large surface pores that requires a thick selective layer to avoid fracture. To solve this problem, we used poly(acrylic acid-co-2-acrylamido-2-methyl propane sulfonic acid) (P(AA-AMPS)) to crosslink PVA to improve the mechanical property of the coating layer. The PVA layer was deposited on to a highly porous PTFE substrate via spray-coating. By optimizing the spray-coating conditions, a thin and defect-free P(AA-AMPS) crosslinked PVA/PTFE composite membrane with a selective layer thickness of 1.1 μm was prepared. The water flux of the composite membrane reached to 256.6 ± 31.3 kg/(m^2 h) at 75 °C with a NaCl rejection rate over 99.9% when desalinating a 3.5 wt.% NaCl solution. The membrane flux is higher than all reported PV desalination membranes.

1. Introduction

The demand for freshwater has been growing continuously with the growth in population and industrial development. It is estimated that 2 billion of people depends on contaminated water in 2021 (Eljaddi et al., 2021; Homaeigohar and Elbahri, 2017; Wei et al., 2021). This raises an increasing demand on water renewable technologies such as seawater desalination (Shannon et al., 2008). Reverse osmosis (RO) dominates the desalination market because of its high desalination efficiency and low energy consumption as compared with the conventional thermal technologies (Abraham et al., 2017; Chen et al., 2009). Other than RO, membrane distillation (MD) and pervaporation (PV) are considered promising membrane technologies for treating concentrated salt solutions to meet the goal of zero-liquid discharge (Camacho et al., 2013; Chiam and Sarbatly, 2013). Due to the dense and hydrophilic surface of PV membranes, they are believed to exhibit much better fouling resistance than MD (Tijing et al., 2015). Nevertheless, most PV membranes show lower water flux than MD membranes under similar operation conditions (Khayet and Matsuura, 2004; Xie et al., 2011; Cho et al., 2011). Hence, it is necessary to develop advanced membrane materials and structures to increase water flux of PV desalination membranes.

Using electrospun nanofibrous membranes as substrates can greatly reduce water vapor transport resistance and consequently increases water flux of composite PV membranes (Selatile et al., 2018). For example, Qin et al. adopted an electrospun polyacrylonitrile (PAN) nanofiber membrane to prepare a composite membrane for PV desalination. An extraordinary high water flux of 238.7 ± 4.1 kg/(m^2 h) were reported when desalinated a 3.5 wt.% NaCl water solution at 80 °C (Qin et al., 2021). However, the electrospinning parameters must be precisely controlled to obtain the desired surface morphologies of the nanofiber substrate (Gopal et al., 2006; Lalia et al., 2013). Moreover, the electrospinning process is typically complicated and time-consuming, which is not conducive to large-scale production.

Among polymeric membranes, porous poly(tetrafluoroethylene) (PTFE) membranes exhibit outstanding chemical stability, high heat resistance, strong hydrophobicity, and high fracture toughness (Astakhov and Shutov, 2007; Shyr et al., 2015). Its large pore size, high porosity and super-hydrophobicity minimize the mass transfer resistance of the support layer. Meng et al. deposited polyvinyl alcohol (PVA) on the PTFE porous support layers by spray-coating. A high water flux of 143.4 ± 8.9 kg/(m^2 h) was obtained at 75 °C using a 3.5 wt.% NaCl solution as feed with a dense layer thickness

* *Corresponding authors.*
E-mail addresses: bcao@mail.buct.edu.cn (B. Cao), zhangrui1@mail.buct.edu.cn (R. Zhang), lipei@mail.buct.edu.cn (P. Li).
https://doi.org/10.1016/j.cherd.2022.01.028

2.6 μm (Meng et al., 2020). However, when the thickness of the PVA dense layer was further reduced, it was fractured during a PV experiment. That was due to the poor mechanical strength of the PVA layer crosslinked by 4-sulfophthalic acid (SPTA). Xue et al. fabricated a series of thin film composite membranes of which the PVA dense layers were crosslinked by three crosslinkers including sulfosuccinic acid (SSA), 4-sulfophthanlic acid (SPTA), and poly(acrylic acid-co-2-acrylamido-2-methyl propane sulfonic acid)(P(AA-AMPS)) (Xue et al., 2020). The fracture pressures of the free standing crosslinked PVA films were 0.122 ± 0.023, 0.054 ± 0.014, and 0.371 ± 0.036 MPa for SSA, SPTA, and P(AA-AMPS) crosslinkers, respectively. Hence, the P(AA-AMPS) crosslinked PVA has the best mechanical property.

Here in this work, we selected a hydrophobic PTFE membrane with micro-sized pores as the substrate. P(AA-AMPS) was used to crosslink PVA that was deposited onto the PTFE membrane to form a PV composite membrane. It is expected that the P(AA-AMPS) crosslinked PVA layer shall have better mechanical strength and maintain its integrity with a thin thickness. A PVA/PTFE composite membrane with much higher water flux can be realized.

2. Experimental

2.1. Materials

PTFE microfiltration membranes with a mean surface pore size of 0.22 μm were bought from Beijing Shenghe Integrity Membrane Science and Technology Development Center (China). PVA (hydrolysis degree: 99.4%) and sodium chloride (NaCl, purity ≥ 99.5%) were purchased from Sinopharm Chemical Reagent Co., Ltd. (China). A 30 wt.% poly (acrylic acid co-2-acrylamido-2-methyl propane sulfonic acid) (P(AA-AMPS)) water solution was got from Sigma-Aldrich. Deionized (DI) water was produced from a lab equipped Millipore ultrapure water system.

2.2. Preparation of the PVA/P(AA-AMPS) coating solution

3 g of PVA polymer powder was mixed with 97 mL of DI water. The solution mixture was mage-stirred at 95 °C for 5 h to obtain a homogeneous solution. After the solution cooled down to room temperature, certain amounts of P(AA-AMPS) (a crosslinker) and 0.1 mol/L sulfuric acid solution (a catalyst) were added consequently to adjust the solution pH to 1.

2.3. Preparation of the PVA/PTFE composite membranes

First, a PTFE film was stuck on top of a glass board by scotch tape. A 0.5 wt.% PVA/P(AA-AMPS) (7:3 w/w) solution was spray on to the PTFE membrane using an airbrush (S120, nozzle diameter 0.2 mm). The included angle between the nozzle and the PTFE substrate was controlled at 80°, the operation pressure was 0.3 MPa, and the distance between the nozzle to the substrate was 10 cm. During spraying, the airbrush traversed through the PTFE surface cyclically at a rate of 4.5 cm s^{-1} till roughly 1 mL of the coating solution was spent. After that, the composite membrane was crosslinked at 100 °C for 15 min.

To tune the size of the PVA droplet, an optical microscope was used to monitor the atomized PVA solution at different spraying pressures. Specifically, a 0.5 wt.% coating solution was sprayed onto a glass board at varied pressures, while other spray coating parameters were unchanged. The mean drop sizes were analyzed using an Image J software.

2.4. Characterization

2.4.1. Morphologies of the membranes

A thermal field emission scanning electron microscope (SEM, JSM-7800F, JEOL Ltd, Japan) was used to determine the cross-section and surface morphologies of the PVA/PTFE composite membranes. Cross-sectional images were obtained by fracturing the composites in liquid nitrogen. The thicknesses of dense PVA selective layers were determined from their cross-sectional SEM images using a Nano Measurer software. All samples were sputter coated with gold before SEM analyses.

2.4.2. ATR-FTIR spectroscopy

The chemical structure of PVA/P(AA-AMPS) was characterized by a Fourier transform infrared spectroscopy (ATR-FTIR, Nicolet 560) to determine the chemical structures of the cross-linked PVA/P(AA-AMPS) polymer. ATR-FTIR spectra of the surface of the composites were obtained with an 8 cm^{-1} resolution in a wavelength range from 650 to 4000 cm^{-1}.

2.4.3. Water swelling properties

Dried self-standing PVA/P(AA-AMPS) and PVA films were first weighed to obtain their dry weights (m_0). Then, the film was immersed in DI water at room temperature for 72 h to reach sorption equilibrium. After that, water on the film surface was gently wipe off and the film was weighted to obtain the wet-weight (m_1). The swelling degree S (%) was calculated by Eq. (1):

$$S = \frac{m_1 - m_0}{m_0} \times 100\% \quad (1)$$

For each film, the measurement was repeated for 3 times to get the average value of S.

2.4.4. Water contact angle

Hydrophilicity of the pristine PVA and PVA/P(AA-AMPS) crosslinked films were compared by measuring their water contact angles (JC2000D, Powereach, China). At least five locations of each sample were measured to get the average value of water contact angle.

2.4.5. Evaluation of the cracking pressure of the composite membranes

The PVA/PTFE composite membrane was placed on a porous metal plate in a dead-end ultrafiltration device (HP4750, STERLITECH Corporation, USA). 100 mL of pure water was poured onto the membrane. Due to the dense structure of the PVA layer, water would be hold at the membrane feed side. By gradually pressurize the feed solution at a speed of 0.01 bar per minute, the PVA layer was cracked eventually indicated by observing water flowing out of membrane permeate side. The pressure corresponding to that moment was recorded as the cracking pressure of the composite membrane.

2.4.6. Gas permeation tests of the PTFE membrane

To estimate the transport resistance of the PTFE membrane to water vapor, a gas (N_2) permeation cell (Fig. 1) was used to record the gas flux determined by a bubble flow meter at elevated transmembrane pressure (Han et al., 2021). The N_2 volume flux was calculated by Eq. (2)

$$Q = \frac{V}{A_1 t_1} \quad (2)$$

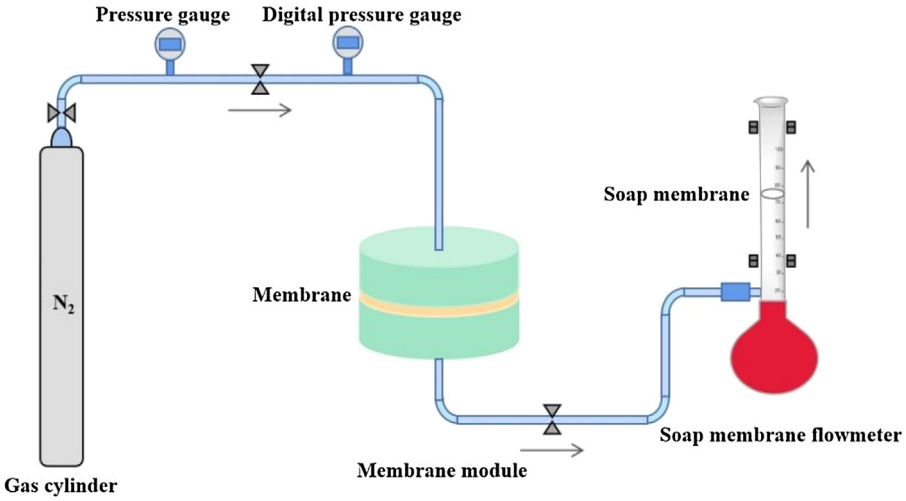

Fig. 1 – A schematic diagram of the gas permeation testing system.

where Q was the gas flux of N_2 (L/(m^2 h)), V the volume of the permeated gas (L), A_1 the effective membrane area (m^2), and t_1 the permeation time (h). Then the resistance was estimated by analyzing the slope of Q and transmembrane pressures.

2.4.7. *Adhesion force of the PVA/PTFE composite membranes*

The adhesion force between the crosslinked PVA layer and the PTFE layer was conducted using a dynamic thermomechanical analysis equipment (DMA Q800, TA, USA). Fig. 2 shows the way to prepare membrane samples. Two faces of the composite membrane were stuck to two glass bars. And the other ends of the glass bars were clamped to the DMA gripper. Temperature of the analysis chamber was controlled at 25 ± 1.2 °C. Test mode was set in controlled force at a rate of 0.2 N min^{-1} until the composite membrane was torn apart. The fracturing strength was used to indicate the adhesion force of the two layers.

2.4.8. *Desalination performance of the PVA/PTFE composite membranes*

The desalination performance of the PVA/PTFE composite membrane was measured by a lab-made PV device shown in Fig. 3. Pressure on the permeate side of the membrane cell was maintained at 100 Pa using a vacuum pump. The effective membrane area was 3.28 cm^2 and a feed solution comprising 3.5 wt.% NaCl was used. In the experiment, the feed solution was preheated to the desired temperature using a water bath, and permeate was collected in a liquid nitrogen cold trap. The average masses of water collected from three experiments was used to calculate the membrane flux using Eq. (3):

$$J_W = \frac{\Delta m}{A_2 t_2} \tag{3}$$

where Δm was the mass of water vapor (kg); A_2 was the effective membrane area (m^2); and t_2 was the experimental time (h).

To estimate salt rejection (R) of the PVA/PTFE Composite Membranes, water in the cold trap was used to wash the back of the composite membranes. A conductivity meter (Oakton Con 110) was used to measure the salt concentrations of feed and permeate solutions. Rejection (R) was calculated using Eq. (4):

$$R = (1 - \frac{C_p}{C_f}) \times 100\% \tag{4}$$

where C_p was the permeate salt concentration and C_f was the feed salt concentration.

3. Results and discussion

3.1. *Characterization of the PVA/P(AA-AMPS) polymers*

The FTIR spectra of the pristine PVA and cross-linked PVA/P(AA-AMPS) polymers are shown in Fig. 4(a). Two peaks (3280 cm^{-1} and 2939 cm^{-1}) were observed in the spectrum of PVA, represented the stretching vibrations of both the −OH and $-CH_2-$ functional groups, respectively. After cross-linked by P(AA-AMPS), the intensity of these two peaks decreased significantly, this proved that some of the hydroxyl groups of PVA had been consumed. Furthermore, PVA/P(AA-AMPS) showed a stronger peak at 1710 cm^{-1} that was attributed to the —C=O stretching vibration of the carboxylic acid. This further proved that PVA have been crosslinked by P(AA-AMPS).

Fig. 4(b) shows that the water swelling degree of the pure PVA film is 1.5 times to that of the crosslinked PVA/P(AA-AMPS) film and the water contact angle increased from 55.26° to 62.51°. These results indicated that the cross-linked PVA was less hydrophilic. Note that, the cracking pressure of the P(AA-AMPS) crosslinked PVA/PTFE membrane was measured to be 0.374 ± 0.031 MPa. After the test, we did SEM test to the film. Cracks formed on the surface as shown in Fig. 4(c_1, c_2). Therefore, the composite membrane would be stable during the PV experiment of which the highest transmembrane pressure was 0.1 MPa.

3.2. *Characterization of the PVA/PTFE composite membranes*

As shown in Fig. 5, the water contact angle of the PTFE support layer was 143.97°, indicating its hydrophobic nature. Since the water contact angle of PVA/P(AA-AMPS) was 62.51°, the big difference in their surface properties caused the difficulty to form strongly bonded layer to layer structure. However, part of the

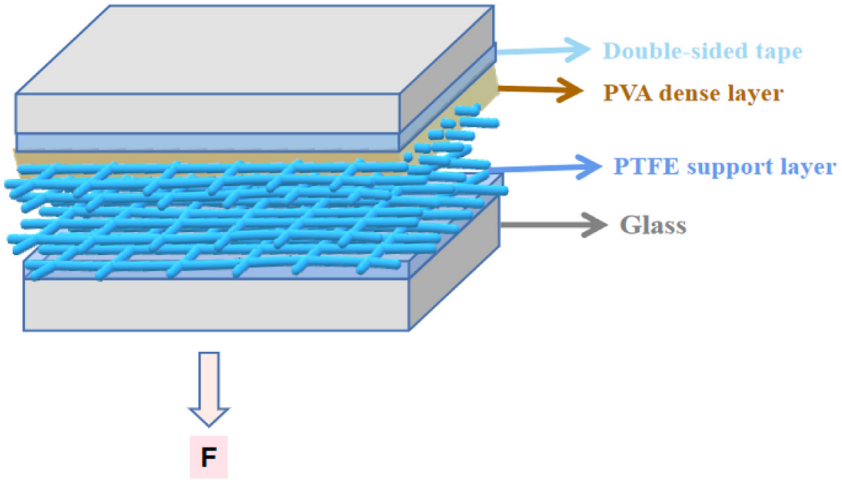

Fig. 2 – A cartoon of preparing membrane sample for testing adhesion force.

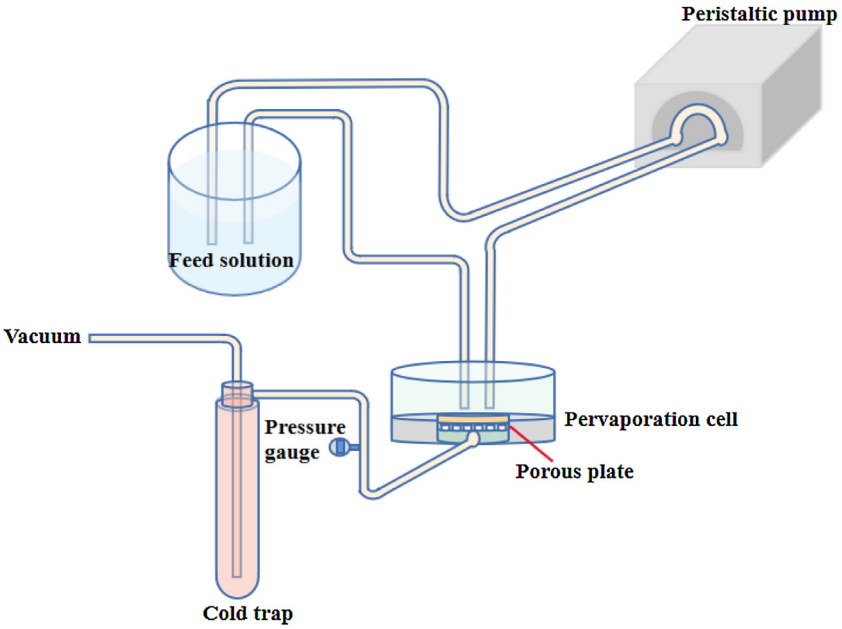

Fig. 3 – A schematic diagram of the pervaporation device (a), and (b) are the sketches of two porous plates: (1) small but more porous substrate; (2) large but less porous substrate.

PVA layer would infiltrate into the PTFE pores by spray-coating and form mechanical-interlock structure as shown in Fig. 6 (Meng et al., 2020). And the adhesion force of the PVA/PTFE composite membrane increased to 0.14 MPa, proved the firmly bonding inter-layer structure. Note that, the composite membrane was teared up in the middle of the PTFE membrane. This indicated that the bonding force between the PVA and PTFE layers was stronger than the bonding force within the PTFE membrane.

The SEM images of the top surfaces and cross sections of the PVA/PTFE composite membranes are shown in Fig. 6(b_1, b_2). The thickness of the PVA layer was 1.1 ± 0.1 μm, and the PVA surface was defect-free (Fig. 6b_1). During the spray-coating process, the droplet sizes are of paramount importance for effective coating. Creech et al. determined nozzle design and application pressure caused the greatest changes in the droplet size (Creech et al., 2017). Therefore, the adjustment of spraying parameters is critical to the impact of the dense layer. The effect of spraying pressure on droplet sizes were detailed studied. The sizes of droplets are impacted by the fluid properties, nozzle type and spray pressure. The droplets form due to the competition between fluid inertia and surface tension. Surface tension and viscosity of the spraying fluid may affect the droplet size. However, the two factors only have limited influence on the size of droplet (Kooij et al., 2018). In this study, a 0.5 wt.% PVA solution was used. Its surface tension was 66.3 mN m^{-1}, slightly lower than the surface tension of deionized water (72.2 mN m^{-1}). The deionized water was sprayed directly on the glass plate to count the median size of the droplets. The pump pressure was adjusted between 0.1 and 0.5 MPa, and a series of microscope photos were taken as shown in Fig. 7(a_1–a_5). The median drop sizes could be found in Supplementary Fig. S1. The median droplets' size was calculated by Eq. (5) (Kooij et al., 2018):

$$D_{50} = C \cdot r \cdot \alpha^{-\frac{1}{6}} We^{-\frac{1}{3}} \quad (5)$$

where $\alpha = \rho_{air}/\rho_{liquid}$, $We = \rho_{liquid} v^2 r/\sigma$, α a density ratio, We a Weber number that reflected the force balance, σ the surface tension, r the radius of the elliptical opening of the conical nozzle, $v = \sqrt{2p/\rho_{liquid}}$ the liquid velocity, p the pressure before

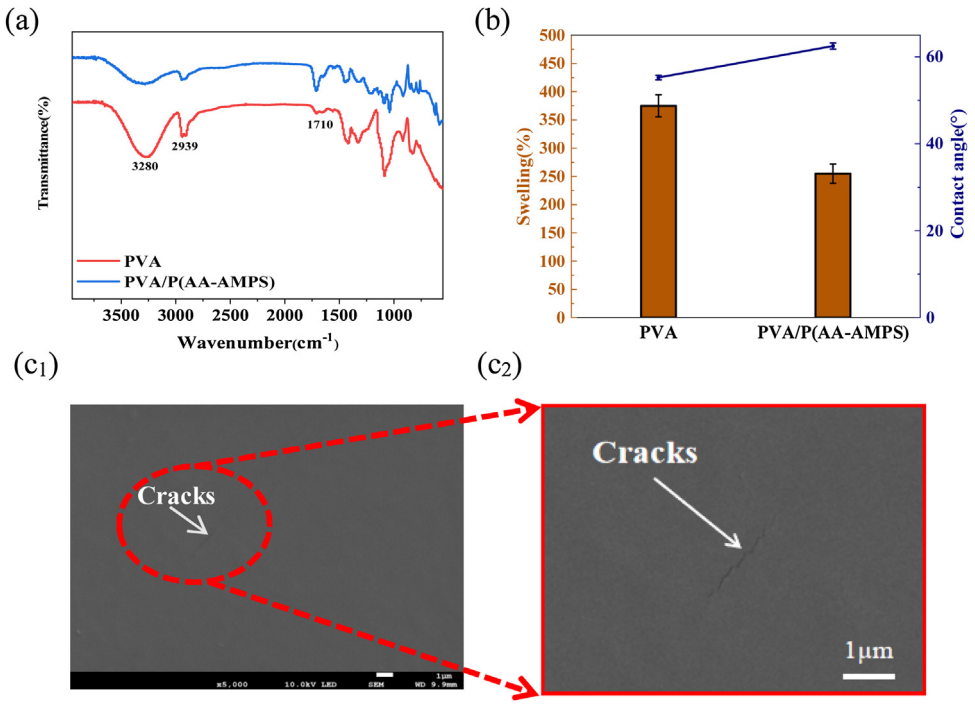

Fig. 4 – (a) FTIR spectra of the PVA and PVA/P(AA-AMPS), (b) swelling degrees and contact angles of PVA and PVA/P(AA-AMPS) films, (c_1, c_2) the surface morphology of the coating after the compression test.

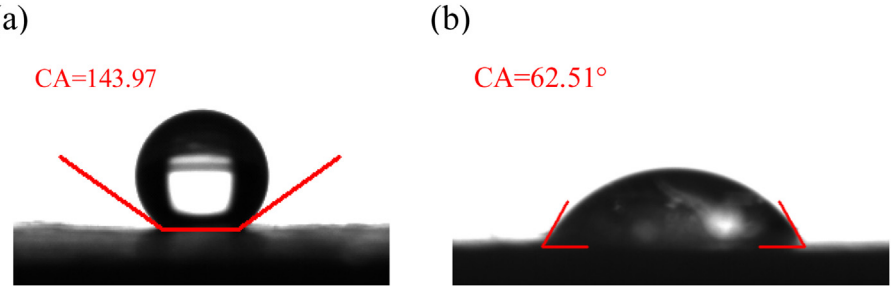

Fig. 5 – Contact angles of (a) the PTFE support layer and (b) the PVA/P(AA-AMPS) films.

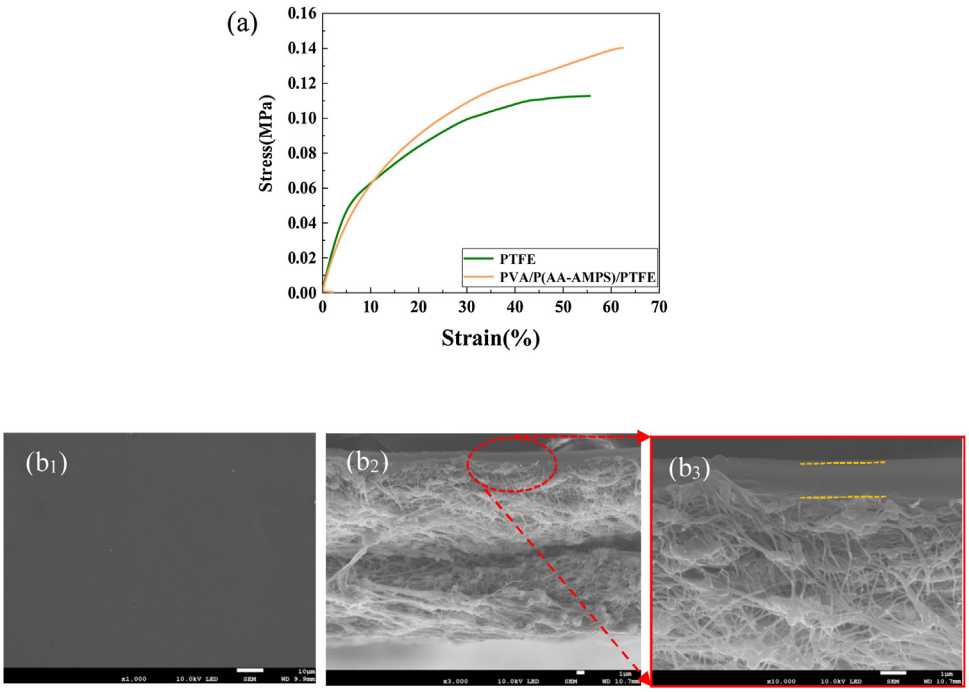

Fig. 6 – (a) The adhesion strength between the PVA/P (AA-AMPS) and PTFE layers in the composite membranes and the adhesion strength of the PTFE membrane itself. SEM images of the top surfaces (b_1) and cross sections of PVA/P (AA-AMPS)/PTFE (b_2, b_3).

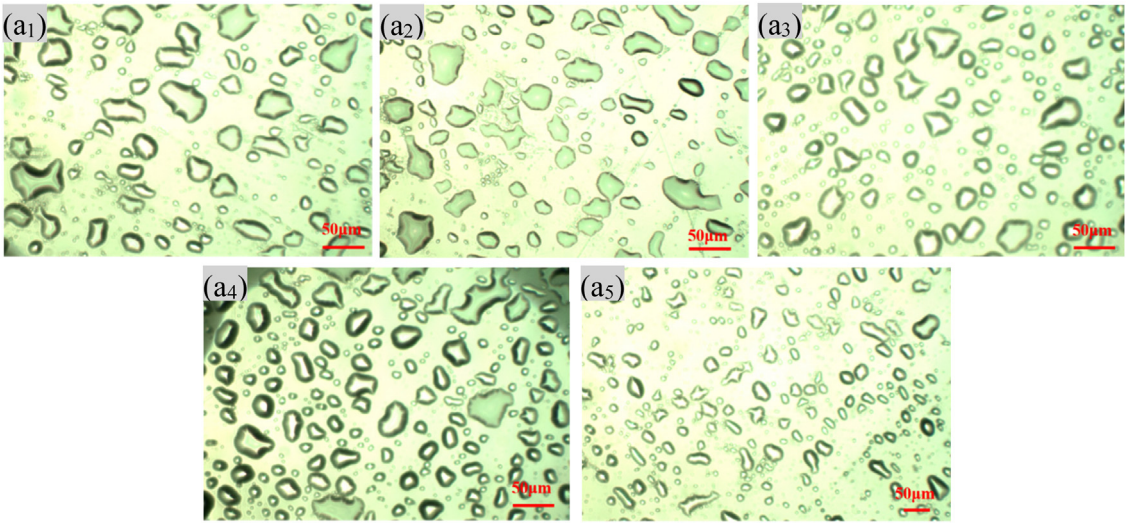

Fig. 7 – Microscope pictures of sprayed droplets under different pressures: pressure is (a_1) 0.1 MPa, (a_2) 0.2 MPa, (a_3) 0.3 MPa, (a_4) 0.4 MPa, (a_5) 0.5 MPa.

Table 1 – The median droplet' size and the scattering angles under different pressures.

p(MPa)	$6.82 \times 10^{-4} p^{-\frac{1}{3}}$ (10^{-5} m)	D_{50}(10^{-5} m)	α(°)
0.1	1.470	1.889	27.88
0.2	1.166	1.521	28.70
0.3	1.019	1.353	33.75
0.4	0.926	1.295	36.54
0.5	0.859	1.204	41.25

and after the nozzle opening. Eq. (5) was transformed into Eq. (6):

$$D_{50} = 6.82 \times 10^{-4} C \cdot p^{-\frac{1}{3}} \quad (6)$$

Here C was a dimensionless constant. The data were plotted by adjusting the pressure according to Eq. (6). Table 1 lists the pressure and median drop size data that were used to calculate C value.

As the spraying pressure increased, the number of droplets increased and the size of the droplets decreased as shown in Fig. 7. The size of the median droplet decreased also, and the value of the dimensionless constant C was 1.29 (Supplementary Fig. S2). Hence, the size of the droplet could be tuned by adjusting the spraying pressure. We also tested the scatterings angle (α) of the spray solution just after they left the conical nozzle under different pressures. The spray droplet size decreased and the scattering angle increased with increased pressure (Fig. 8a). The fixed spraying distance d is 10 cm, and measured the diameter l of the circle sprayed on the glass plate (Fig. 8b). α is calculated by the following Eq. (7):

$$\alpha = 2\theta = arctan\frac{l}{2d} \quad (7)$$

The results are shown in Table 1. As the pressure increases, the scattering angles also increases. At a high spraying pressure, the flow rate of the spray solution increases (Fig. 8c). According to the Bernoulli's equation, this cause the pressure, P_1, decreases. Hence, the increment in ΔP results in an increase in the amount of PV solution fed into the spray gun, and thus an increase in the discharge liquid. Since the increase in pressure is conducive to the atomization of the droplets, the scattering angle of the atomized solution increases.

When the spraying pressure is low, the droplet size is big, the scattering angle is small. Unevenly distributed PVA droplets will be deposited on top of the PTFE membrane and forms coarse PVA surface (Fig. 8d_1). On the other hand, at high spraying pressure, although the PVA solution is atomized effectively, the airflow will be too strong and blow away the PVA droplets on the PTFE surface and cause the formation of defects (Fig. 8d_3). Therefore, a moderate pressure of 0.3 MPa is selected and a defect-free and flat PVA layer of 1 μm forms (Fig. 8d_2).

3.3. *Desalination performances*

Fig. 9(a) shows the effect of feed temperature on the pervaporation desalination performance of the PVA/P(AA-AMPS)/PTFE composite membrane with a PVA layer thickness of 1.1 ± 0.1 μm. The water flux reached to 256.6 ± 31.3 kg/(m^2 h) at 75 °C with a high salt rejection of 99.9%, while the lowest water flux was 91.7 ± 4.6 kg/(m^2 h) at 45 °C. The reason was that the driving force for water transport increased with temperature, and the water diffusivity increased also. As illustrated in Fig. 9(c), we found that the porous metal pad under the PV composite membrane also had significant impact on membrane flux. Using a metal pad with small pore sizes but more pores could increase the membrane flux by 20.9%. This is reasonable since the lateral mass transfer distance of water molecules on the perforated plate (1) becomes smaller, and the water molecules are not easy to accumulate and can diffuse in time, thereby increasing the water flux.

The long-term desalination performance of the PVA/P(AA-AMPS)/PTFE composite membrane using a 3.5 wt.% NaCl solution as the feed at 75 °C was tested (Fig. 9b). After 720 min of experiment, the water flux dropped from 248.7 kg/(m^2 h) to 181.1 kg/(m^2 h), the conductivity of the permeate solution was maintained below 5 μs/cm, and the salt rejections were all higher than 99.9%. The decrease in water flux could be attributed to the formation of salt scales on the selective layer surface (Fig. 9d_1), which blocked part of the water transfer channel, and thus increased the resistance of mass transferring. However, these salt scales could be easily washed off. As shown in Fig. 9(d_2), the surface of the composite membrane was washed with deionized water for 1 h, salt scales disappeared. There were no remarkable differences in mem-

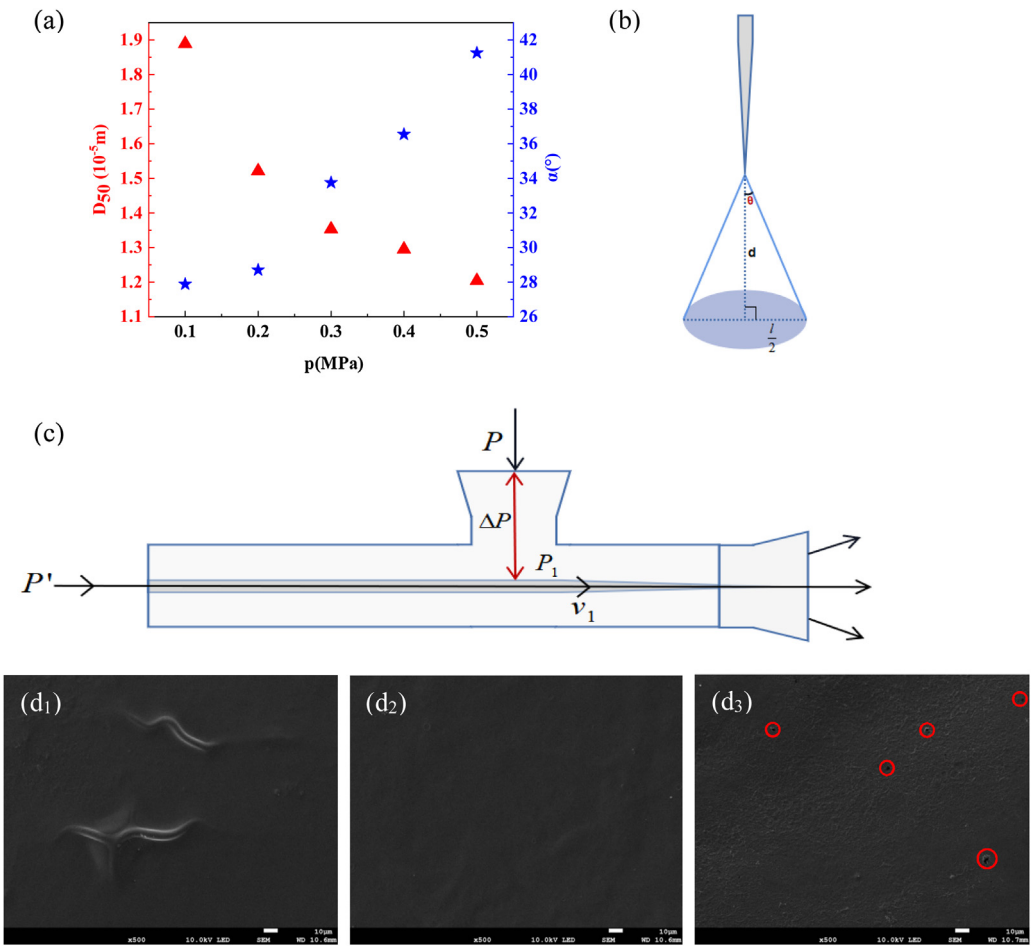

Fig. 8 – (a) Correspondence between pressure and D_{50}. (b) Schematic representation of the breakup mechanism for the conical nozzle. (c) Schematic diagram of spray gun principle. SEM images of film surface under different pressure spraying conditions: pressure is (d_1) 0.1 MPa, (d_2) 0.3 MPa, (d_3) 0.5 MPa.

Table 2 – Comparison of the water permeance and permeability of the PVA layer.

Membrane type	Feed temperature (°C)	Vacuum pressure (kPa)	Water flux (kg/(m^2 }Diff126h)	Salt rejection (%)	Dense layer thickness (μm)	Water permeance (10^4 GPU)	Water permeability (10^4 Barrer)	Reference
S-PVA/PTFE	75	0.1	143.4	99.9	2.6	17.7	46.0	Meng et al. (2020)
S-PVA/PVDF/PTFE	70	0.1	83.4	99.9	2.3	17.1	39.4	Meng et al. (2019)
Mxene/PAN	65	0.4	85.4	99.5	0.06	12	7.2	Liu et al. (2018)
S-PVA/PAN	70	0.1	46.3	99.5	0.8	26.1	21.4	Liang et al. (2018)
S-PVA/PTFE	75	0.1	256.6	99.9	1.1	41.3	45.4	This work

Table 3 – Comparison of desalination properties between PVA/P(AA-AMPS)/PTFE composite membrane fabricated in this work and other composite membranes reported in the literature.

Membrane material	Feed temperature (°C)	Thickness (μm)	NaCl (ppm)	Flux (kg/(m^2 h))	Rejection (%)	Reference
Graphene oxide/polyacrylonitrile	70	–	35,000	46.1	99.8	Liang et al. (2015)
Graphene oxide	90	0.4	35,000	48.4	99.7	Xu et al. (2016)
Graphene oxide/chitosan	81	10–13	100,000	27.6	99.99	Qian et al. (2018a,b)
Graphene oxide/a-Al_2O_3	90	1.6	35,000	20.1	99.9	Qian et al. (2018a,b)
MXene/PAN	65	0.06	35,000	85.4	99.5	Liu et al. (2018)
Maleic acid-MXene/polyamide	65	0.03	35,000	72.4	99.6	Ding et al. (2020)
S-PVA/PSF	70	1.12	35,000	60.8	99.8	Li et al. (2018)
S-PVA/PAN	70	0.8	35,000	46.3	99.5	Liang et al. (2018)
P(AA-AMPS)-PVA/PAN	75	0.73	35,000	211.4	99.8	Xue et al. (2020)
S-PVA/PTFE	75	1.1	35,000	256.6	99.9	This work

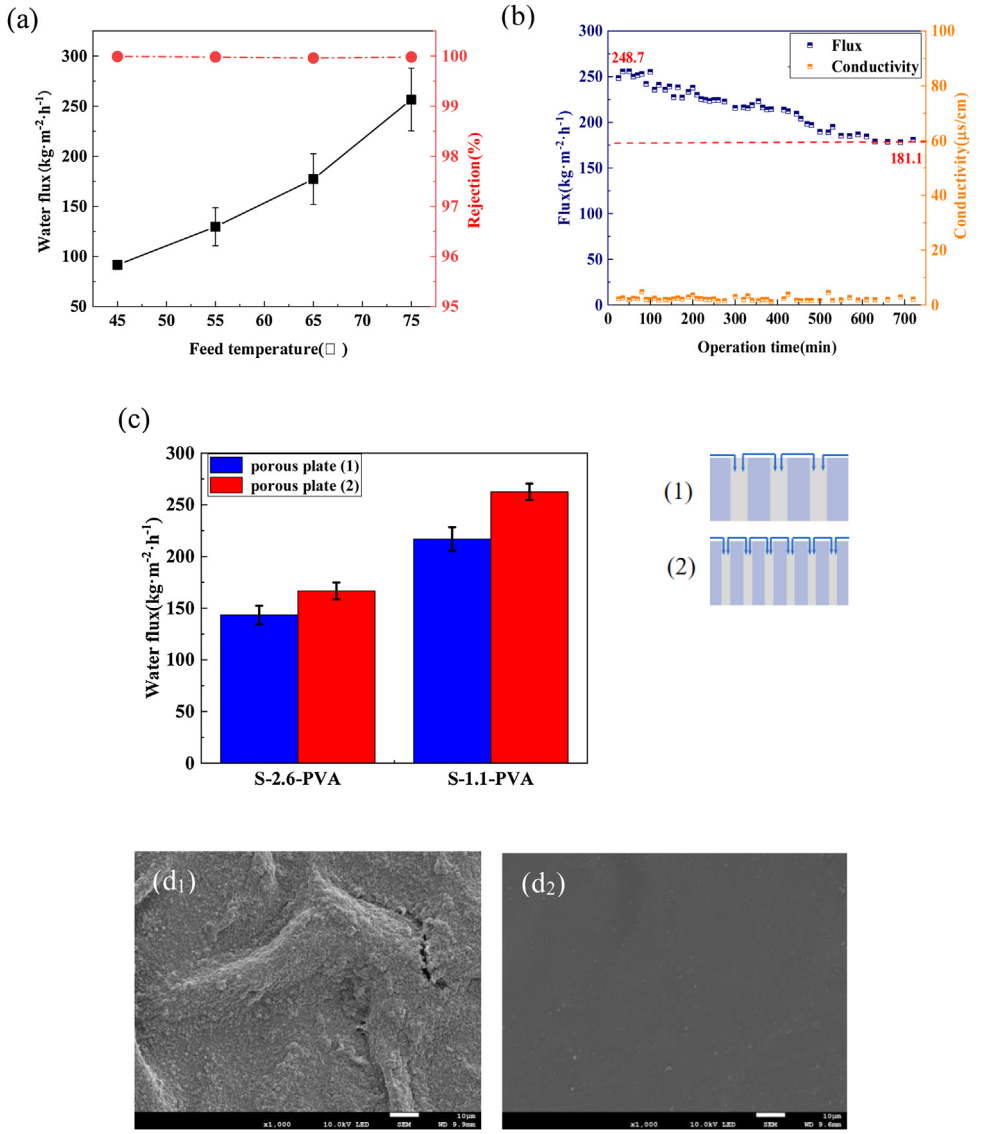

Fig. 9 – (a) Effect of feed temperature on water flux and rejection (feed solution: 3.5 wt.% NaCl, the thickness of PVA/P (AA-AMPS) layer:1.1 ± 0.1 μ m); Long-term desalination performance (b); (c) The influence of porous plate on the water flux and rejection of PV (feed solution: 3.5 wt.% NaCl, operation temperature: 75 °C); Surface SEM images after tests (d_1) and being washed with DI water for 1 h (d_2) of the PVA/P(AA-AMPS)/PTFE membrane (feed solution: 3.5 wt.% NaCl, operation temperature: 75 °C).

brane morphology without any visible cracks, pinholes or other defects, the water flux could also be restored. Therefore, the PV composite film had good long-term operation stability.

As listed in Table 2, we calculated water permeance and permeability of the PVA layer for the PVA/PTFE membrane (Supporting Information) and compared with some literature reported data. For S-PVA/PTFE and PVA/PTFE composite membranes, even though their PVA layers have similar water permeability, the water permeance of our PVA/PTFE composite membrane is much higher. This is mainly because the dense layer of PVA/P(AA-AMPS) is thinner, making the mass transfer resistance of the dense layer lower than that of the S-PVA/PTFE composite membrane.

3.4. *Comparison of desalination properties of representative PV membranes*

In Table 3, the water fluxes of the composite membrane fabricated in this work were compared with other high-performance PV desalination membranes reported in the literature, the S-PVA/PTFE composite membrane had the highest water fluxes. The dramatically improved water fluxes could be attributed to three reasons: first, the P(AA-AMPS) crosslinked PVA film had good mechanical strength and could maintain its integrity at a thickness of 1.1 μm; secondly, the reduction of the thickness of the PVA layer reduced the mass transfer resistance, and increased the water fluxes; thirdly, attributing to the larger surface pores (0.22 μm) of the PTFE substrate, the transport resistance of the porous region was lower and thereby increased the water flux.

4. Conclusions

We prepared a series of P(AA-AMPS) crosslinked PVA/PTFE composite membranes. Benefit from the good mechanical property of the P(AA-AMPS) crosslinked PVA film and the optimized spray-coating process, the thickness of the PVA layer have been reduced to 1.1 μm and the composite membrane could maintain it integrity during the PV desalination experi-

ments. The water fluxes reached 256.6 kg/(m^2 h) with a NaCl rejection of 99.9% using a 3.5 wt.% NaCl solution at a 100 Pa vacuum and a temperature of 75 °C. The performance outplays existing PV desalination membranes to our best knowledge.

Data availability

All data included in this study are available upon request by contact with the corresponding author.

Conflict of interest

There is no conflict of interest with any other groups.

Acknowledgement

This research is funded by National Key R&D Program of China (2021YFC210201-3).

Appendix A. Supplementary data

Supplementary material related to this article can be found, in the online version, at doi:https://doi.org/10.1016/j.cherd.2022.01.028.

References

Abraham, J., Vasu, K.S., Williams, C.D., Gopinadhan, K., Su, Y., Cherian, C.T., Dix, J., Prestat, E., Haigh, S.J., Grigorieva, I.V., Carbone, P., Geim, A.K., Nair, R.R., 2017. Tunable sieving of ions using graphene oxide membranes. Nat. Nanotechnol. 12, 546–550.

Astakhov, E.Y., Shutov, A.A., 2007. Porous polytetrafluoroethylene film. Tech. Phys. Lett. 33, 228–230.

Camacho, L., Dumée, L., Zhang, J., Li, J.-d., Duke, M., Gomez, J., Gray, S., 2013. Advances in membrane distillation for water desalination and purification applications. Water 5, 94–196.

Chen, C., Yang, Q.-H., Yang, Y., Lv, W., Wen, Y., Hou, P.-X., Wang, M., Cheng, H.-M., 2009. Self-assembled free-standing graphite oxide membrane. Adv. Mater. 21, 3007–3011.

Chiam, C.-K., Sarbatly, R., 2013. Vacuum membrane distillation processes for aqueous solution treatment—a review. Chem. Eng. Process. Process Intensif. 74, 27–54.

Cho, C.H., Oh, K.Y., Kim, S.K., Yeo, J.G., Sharma, P., 2011. Pervaporative seawater desalination using NaA zeolite membrane: mechanisms of high water flux and high salt rejection. J. Membr. Sci. 371, 226–238.

Creech, C.F., Henry, R.S., Fritz, B.K., Kruger, G.R., 2017. Influence of herbicide active ingredient, nozzle type, orifice size, spray pressure, and carrier volume rate on spray droplet size characteristics. Weed Technol. 29, 298–310.

Ding, M., Xu, H., Chen, W., Yang, G., Kong, Q., Ng, D., Lin, T., Xie, Z., 2020. 2D laminar maleic acid-crosslinked MXene membrane with tunable nanochannels for efficient and stable pervaporation desalination. J. Membr. Sci. 600.

Eljaddi, T., Mendez, D.L.M., Favre, E., Roizard, D., 2021. Development of new pervaporation composite membranes for desalination: theoretical and experimental investigations. Desalination 507.

Gopal, R., Kaur, S., Ma, Z., Chan, C., Ramakrishna, S., Matsuura, T., 2006. Electrospun nanofibrous filtration membrane. J. Membr. Sci. 281, 581–586.

Han, W., Zhang, C., Zhao, M., Yang, F., Yang, Y., Weng, Y., 2021. Post-modification of PIM-1 and simultaneously in situ synthesis of porous polymer networks into PIM-1 matrix to enhance CO_2 separation performance. J. Membr. Sci. 636.

Homaeigohar, S., Elbahri, M., 2017. Graphene membranes for water desalination. NPG Asia Mater. 9, e427–e427.

Khayet, M., Matsuura, T., 2004. Pervaporation and vacuum membrane distillation processes: modeling and experiments. AIChE J. 50, 1697–1712.

Kooij, S., Sijs, R., Denn, M.M., Villermaux, E., Bonn, D., 2018. What determines the drop size in sprays? Phys. Rev. X 8.

Lalia, B.S., Kochkodan, V., Hashaikeh, R., Hilal, N., 2013. A review on membrane fabrication: structure, properties and performance relationship. Desalination 326, 77–95.

Li, Q., Cao, B., Li, P., 2018. Fabrication of high performance pervaporation desalination composite membranes by optimizing the support layer structures. Ind. Eng. Chem. Res. 57, 11178–11185.

Liang, B., Zhan, W., Qi, G., Lin, S., Nan, Q., Liu, Y., Cao, B., Pan, K., 2015. High performance graphene oxide/polyacrylonitrile composite pervaporation membranes for desalination applications. J. Mater. Chem. A 3, 5140–5147.

Liang, B., Li, Q., Cao, B., Li, P., 2018. Water permeance, permeability and desalination properties of the sulfonic acid functionalized composite pervaporation membranes. Desalination 433, 132–140.

Liu, G., Shen, J., Liu, Q., Liu, G., Xiong, J., Yang, J., Jin, W., 2018. Ultrathin two-dimensional MXene membrane for pervaporation desalination. J. Membr. Sci. 548, 548–558.

Meng, J., Li, P., Cao, B., 2019. High-flux direct-contact pervaporation membranes for desalination. ACS Appl. Mater. Interfaces 11, 28461–28468.

Meng, J., Lau, C.H., Xue, Y., Zhang, R., Cao, B., Li, P., 2020. Compatibilizing hydrophilic and hydrophobic polymers via spray coating for desalination. J. Mater. Chem. A 8, 8462–8468.

Qian, X., Li, N., Wang, Q., Ji, S., 2018a. Chitosan/graphene oxide mixed matrix membrane with enhanced water permeability for high-salinity water desalination by pervaporation. Desalination 438, 83–96.

Qian, Y., Zhou, C., Huang, A., 2018b. Cross-linking modification with diamine monomers to enhance desalination performance of graphene oxide membranes. Carbon 136, 28–37.

Qin, D., Zhang, R., Cao, B., Li, P., 2021. Fabrication of high-performance composite membranes based on hierarchically structured electrospun nanofiber substrates for pervaporation desalination. J. Membr. Sci. 638.

Selatile, M.K., Ray, S.S., Ojijo, V., Sadiku, R., 2018. Recent developments in polymeric electrospun nanofibrous membranes for seawater desalination. RSC Adv. 8, 37915–37938.

Shannon, M.A., Bohn, P.W., Elimelech, M., Georgiadis, J.G., Marinas, B.J., Mayes, A.M., 2008. Science and technology for water purification in the coming decades. Nature 452, 301–310.

Shyr, T.-W., Chung, W.-C., Lu, W.-L., Lin, A.-J., 2015. Unusually high temperature transition and microporous structure of polytetrafluoroethylene fibre prepared through film fibrillation. Eur. Polym. J. 72, 50–63.

Tijing, L.D., Woo, Y.C., Choi, J.-S., Lee, S., Kim, S.-H., Shon, H.K., 2015. Fouling and its control in membrane distillation—a review. J. Membr. Sci. 475, 215–244.

Wei, H., Zhao, S., Zhang, X., Wen, B., Su, Z., 2021. The future of freshwater access: functional material-based nano-membranes for desalination. Mater. Today Energy 22.

Xie, Z., Hoang, M., Duong, T., Ng, D., Dao, B., Gray, S., 2011. Sol–gel derived poly(vinyl alcohol)/maleic acid/silica hybrid membrane for desalination by pervaporation. J. Membr. Sci. 383, 96–103.

Xu, K., Feng, B., Zhou, C., Huang, A., 2016. Synthesis of highly stable graphene oxide membranes on polydopamine functionalized supports for seawater desalination. Chem. Eng. Sci. 146, 159–165.

Xue, Y.L., Huang, J., Lau, C.H., Cao, B., Li, P., 2020. Tailoring the molecular structure of crosslinked polymers for pervaporation desalination. Nat. Commun. 11, 1461.